Dynamic ice loads for offshore wind support structure design

Hammer, Tim C.; Willems, Tom; Hendrikse, Hayo

DOI
10.1016/j.marstruc.2022.103335

Publication date
2023

Document Version
Final published version

Published in
Marine Structures

Marine Structures 87 (2023) 103335

Contents lists available at ScienceDirect

Marine Structures

journal homepage: www.elsevier.com/locate/marstruc

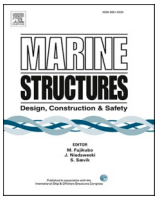

Dynamic ice loads for offshore wind support structure design

Tim C. Hammer [a,b,*], Tom Willems [b], Hayo Hendrikse [a]

[a] Delft University of Technology, Faculty of Civil Engineering and Geosciences, Stevinweg 1, 2628 CN, Delft, the Netherlands
[b] Siemens Gamesa Renewable Energy, Prinses Beatrixlaan 800, 2595 BN, Den Haag, the Netherlands

ARTICLE INFO

Keywords:
Ice-structure interaction
Ice-induced vibrations
Frequency lock-in
Intermittent crushing
Monopile
Multi-modal interaction

ABSTRACT

For offshore wind farms which are planned in sub-arctic regions like the Baltic Sea and Bohai Bay, support structure design has to account for load effects from dynamic ice-structure interaction. There is relatively high uncertainty related to dynamic ice loads as little to no load- and response data of offshore wind turbines exposed to drifting ice exists. In the present study the potential for the development of ice-induced vibrations for an offshore wind turbine on monopile foundation is experimentally investigated. The experiments aimed to reproduce at scale the interaction of an idling and operational 14 MW turbine with ice representative of 50-year return period Southern Baltic Sea conditions. A real-time hybrid test setup was used to allow the incorporation of the specific modal properties of an offshore wind turbine at the ice action point, as well as virtual wind loading. The experiments showed that all known regimes of ice-induced vibrations develop depending on the magnitude of the ice drift speed. At low speed this is intermittent crushing and at intermediate speeds is 'frequency lock-in' in the second global bending mode of the turbine. For high ice speeds continuous brittle crushing was found. A new finding is the development of an interaction regime with a strongly amplified non-harmonic first-mode response of the structure, combined with higher modes after moments of global ice failure. The regime develops between speeds where intermittent crushing and frequency lock-in in the second global bending mode develop. The development of this regime can be related to the specific modal properties of the wind turbine, for which the second and third global bending mode can be easily excited at the ice action point. Preliminary numerical simulations with a phenomenological ice model coupled to a full wind turbine model show that intermittent crushing and the new regime result in the largest bending moments for a large part of the support structure. Frequency lock-in and continuous brittle crushing result in significantly smaller bending moments throughout the structure.

1. Introduction

Today about 2 GW offshore wind capacity is installed in the Baltic Sea, while WindEurope estimates that up to 85 GW could be deployed by 2050 [1]. Offshore wind turbines built in sub-arctic regions like the Baltic Sea and the Bohai Bay are facing one main distinguishing challenge: sea ice.

Structures in sub-arctic regions need to be designed to withstand ice loads induced by different ice features. Structures are typically exposed to level, rafted, and ridged ice. Those ice types, depending on ice properties like thickness, drift speed and floe size, can cause severe local and global loads on the structure. Ice loads and corresponding structural response are typically driven by failure modes of the

* Corresponding author. Delft University of Technology, Faculty of Civil Engineering and Geosciences, Stevinweg 1, 2628 CN, Delft, the Netherlands.
E-mail address: T.C.Hammer@tudelft.nl (T.C. Hammer).

https://doi.org/10.1016/j.marstruc.2022.103335
Received 22 December 2021; Received in revised form 30 September 2022; Accepted 6 November 2022
Available online 19 November 2022

ice: ice bending or buckling leads to moderate loads, while structures exposed to crushing ice experience higher loads. For vertically sided structures, like offshore wind turbines with monopile foundations, design focusses on global loads caused by crushing ice mainly.

Crushing of ice and associated loads depend highly on the structural motion during interaction. The non-linear processes involved can cause ice-induced vibrations (IIV), which have resulted in structural damage and near critical incidents for offshore structures in the past. Experience with bottom-founded jacket structures excited by crushing ice in the Cook Inlet (Alaska) and in the Bohai Bay (China), showed that dynamic ice loads can result in critical conditions for ultimate strength and fatigue for multi-leg structures [2–4]. To their surprise, the crew of the caisson-based drilling platform Molikpaq experienced ice-induced vibrations during its deployment in the Beaufort Sea where an ice event caused concern for the risk of sand-core liquefaction [5]. Adding to the observations of ice-induced vibrations of multileg and wide structures, also slender single-interface structures like caisson-based lighthouses and steel channel markers (both installed in the Baltic Sea) have experienced ice-induced vibrations [6–8]. No full-scale observations of ice-induced vibrations for offshore wind turbines on monopile foundations have been reported to date. This is mainly because of recent, relatively mild winters in Europe and few structures on monopiles so far have been installed and monitored at locations where sea ice can develop.

Over the past decades it has become clear that structures with a relatively high 'compliance' are more prone to severe ice-induced vibrations [9]. In general the relative importance of structural stiffness at the ice action point, oscillating mass and damping of structures is not known yet. Comparing offshore wind turbines with lighthouses, channel markers, and oil- and gas platforms which have experienced ice-induced vibrations in the past, it is to be expected that in similar ice conditions a more severe dynamic response will develop for an offshore wind turbine [10]. The reason for that is the relatively high compliance and low damping of the wind turbines, especially during idling.

For this reason, the applicable design standard IEC61400-3-1 [11] emphasizes the importance of considering dynamic ice-structure interaction for offshore wind support structure design in sub-arctic regions. Three different approaches to consider dynamic ice loads in the support structure design are proposed:

1. Analysis of ice action data (statistical data) from similar structures in similar ice conditions;
2. Application of sufficiently advanced numerical models including the dynamics of the structure, the dynamics of the ice and their interaction;
3. Usage of measurements (model testing).

The challenge with these approaches is that data from similar structures in similar ice conditions does not exist. Numerical models are being used, but these have not been extensively validated for their capacity to predict the interaction between ice and offshore wind turbines owing to the same shortage of data. Model-scale experiments which did target offshore wind encountered challenges related to scaling. This resulted in ice buckling to develop rather than crushing in the tests with vertical structures [12,13]. Other experiments dedicated to offshore wind turbines did not consider the structural dynamics, treating the structure as rigid [14] or only partly focussing on the first global bending mode of the turbine [15].

In the present study we introduce the results from ice tank tests aimed to reproduce the interaction of a 14 MW offshore wind turbine in ice conditions representative of severe conditions (50-year return period) in the Southern Baltic Sea. The goal of the experiments was to answer the question: which regimes of ice-induced vibrations can develop for an offshore wind turbine in these conditions? Both an idling and operational turbine were tested using a real-time hybrid test setup to obtain some insight into the effect of combined wind and ice loading on the development of ice-induced vibrations. Preliminary numerical simulations using a phenomenological ice model coupled to a detailed wind turbine model were performed to obtain insight into the relevance of the experimentally identified ice-induced vibration regimes for design of offshore wind support structures.

The experimental campaign is first briefly introduced, where reference is made to a more detailed description in Ref. [16]. Data from the campaign used in this paper are publicly available from Ref. [17]. The ice and wind turbine model used for the numerical simulations are introduced with reference to existing literature. The experimental results are presented with a focus on the regimes of ice-induced vibrations that developed during the tests. A comparison between idling and operational cases is made to assess the effect of wind loading on the interaction of the structure with the ice. This is followed by the numerical results where first the ability of the model to qualitatively capture the experimentally observed ice-induced vibration regimes is demonstrated. Second, bending moments over the height of the support structure are analysed to assess the relative importance of the different regimes of ice-induced vibrations for design. Finally, the discussion covers generalization of the results and limitations of the experiments.

2. Methods

In this section details of the experimental campaign relevant for the analysis presented in the present study are introduced. The tests reported herein were part of a larger test campaign in the SHIVER project which is described in detail in Ref. [16]. The ice model and structural model used for the numerical simulations are introduced as well.

2.1. Experimental campaign

In June 2021 basin tests were conducted at the Aalto Ice and Wave Tank aimed to reproduce the dynamic interaction between a drifting ice sheet and an offshore wind turbine on monopile foundation. The experimental setup consisted of a real-time hybrid setup combining physical and numerical components thereby allowing to program any type of structural model and focussing only on the interaction of the structure at the point of contact with the ice [18]. That way, the unique modal characteristics of the offshore wind

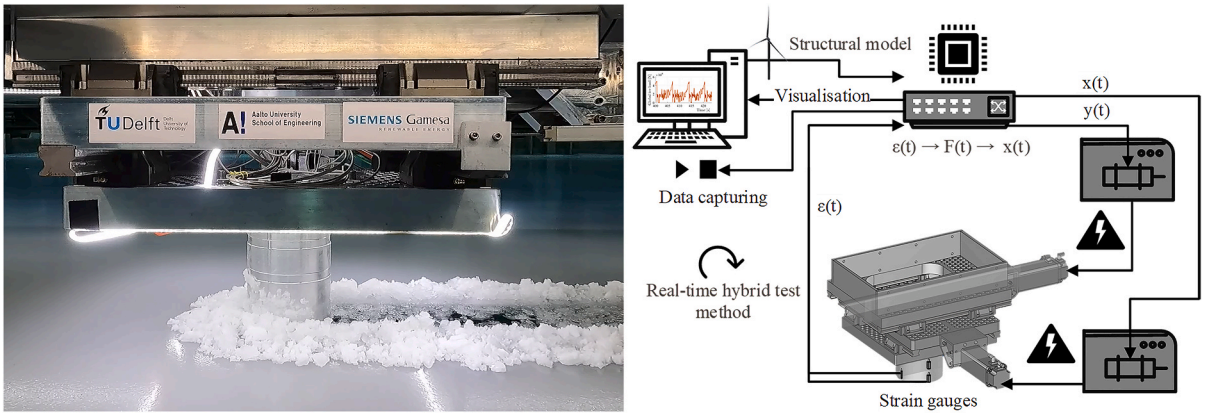

Fig. 1. Left: Photograph of the real-time hybrid test setup during testing, showing the cylindrical pile interacting with the ice. Right: Schematic overview of the real-time hybrid test setup [18].

turbine could be preserved in the model-scale setup.

A photograph of the setup in the basin is shown in Fig. 1, combined with a schematic overview of the different components. An aluminum, vertical cylindrical pile with a diameter of 200 mm penetrated the ice sheet. The pile matched the displacements of the simulated structure at the ice action point. Ice loads were identified from pile strains measured with strain gauges located above the ice action point. The response of the simulated structure to the measured ice loads was numerically simulated on a micro-controller. The calculated structural displacement at the ice action point was applied to the pile by bi-directional linear actuators. The pile displacements were measured by displacement sensors.

The real-time hybrid test setup was mounted to a carriage. The carriage was mounted to a bridge spanning the ice tank. Ice drift was simulated by moving the carriage along the bridge with pre-defined speeds. The resulting apparent ice drift (simulated by the moving carriage and the stationary ice sheet) was then opposite to the carriage movement direction. Herein we describe movement of the carriage as ice drift. The real-time hybrid test setup is described as the structure. The measured pile displacements relative to the carriage supporting the real-time hybrid test setup are described as the structural displacements.

During the tests, the global ice forces and structural responses were measured with load cells, strain gauges, accelerometers, and displacement sensors as further described in Ref. [18]. The analyses presented in the present study use the unfiltered measured global ice force and structural displacement.

2.1.1. Model ice and test characteristics

The model ice was created by spraying a fine mist of a water-ethanol mixture on a thin layer of initial ice, according to the following procedure: 1) Lower the tank temperature to −10 °C. 2) Remove the ice that has formed on the tank surface. 3) Re-freeze the water surface for 20 min, forming a smooth, thin layer of ice. 4) Spray mist at −10 °C for 180 min, forming a layer of sprayed ice of 20 mm. 5) Harden the ice at −11 °C for a total of 150 freezing-degree-hours. The spraying water and the water in the ice tank had an ethanol content of 0.3%. The spraying process resulted in a fine grain structure that captured the ethanol in small pockets.

During test days the ice was kept at −11 °C to obtain ice with a high bending- and crushing strength, and effective modulus, which promoted crushing failure to prevail. The ice material properties were measured according to the International Towing Tank Conference recommended procedures and guidelines [19]. The flexural (σ_f) and compressive (σ_c) strengths of the ice were measured at the end of each test day. It is noted that there is uncertainty with respect to the compressive strength values as the ice samples tested failed in a combination of bending and compression. This may have yielded lower values than representative for the ice. An analysis on this topic and the behaviour of the cold model ice in Ref. [20] shows that the effective strength during indentation, defined as the global load divided by the contact area, was about 1.5 MPa, though this larger value may also be related to different confinement compared to the standard ice property test. The ice thickness was measured after each test run at four equally spaced locations along the channel created by the structure and is given as mean value h_{mean}.

The test data used in this study are summarised in Table 1 and can be found in Ref. [17]. Test data are from four runs on two different test days (June 21, 2021 and June 23, 2021). Specifically, the data used are from test ID 589, 590, 593 and 601 for an idling turbine (run 3 and run 5 on June 21, 2021), and test ID 620, 621, 624, 627, 660 and 661 for an operational turbine (run 8 and run 9 on June 23, 2021). For some ice drift speeds, tests had been captured in two test IDs. Those two test IDs have been merged in this study. Merged timeseries are indicated in the figures accordingly.

2.1.2. Scaling and structural model

For this test campaign, the choice was made to not scale time, as the time-dependent behaviour of the ice in the tank could not be easily controlled and was not known in the planning phase of the experiments. In addition, the waterline displacements of the test structures were kept scale invariant, by which we mean that the displacements in the basin are equal in magnitude to those in full-scale. Ziemer proposed and discussed the merits of this type of scaling approach for crushing in a recent analysis [21]. To achieve

Table 1
Overview of tests from the experimental campaign considered in this study. The air temperature T, the ice compressive and flexural strength (σ_c and σ_f, respectively), and measured ice thickness per run h_{mean} are listed.

TURBINE STATE	TEST ID	ICE DRIFT SPEED	TEST DAY AND RUN	T	σ_c	σ_f	h_{mean}	WIND
		[mm s^{-1}]		[°C]	[kPa]	[kPa]	[mm]	
Idling			June 21, 2021	−11 °C	579	526		–
	589,590,593	Ramp,5,20	Run 3				31	
	601	40	Run 5				32	
Operational			June 23, 2021	−11 °C	658	470		Fig. 3
	(620 + 660), (621 + 661),624	(Ramp), (5),20	Run 8				35	
	627	40	Run 9				37	

structural deformations similar to full-scale, a mass scaling factor λ_m was applied to each mode of the structural models, affecting the mass (m), stiffness (k) and damping (c) of the structure. The scaling factor was determined based on the ratio between full-scale (FS) and model-scale (MS) mean brittle crushing load $\overline{F}$ at 0.1 m s^{-1} indentation speed:

$$\lambda_m = \lambda_k = \lambda_c = \frac{\overline{F}_{FS}}{\overline{F}_{MS}} \tag{3}$$

This approach ensures that the displacement of the structure in model-scale is equal to the full-scale displacement. Geometric scaling was relaxed, with the main focus being to assure crushing failure without flexural deformation. This was achieved with a structural diameter of 200 mm and target ice thickness in the range of 30 mm. A more detailed discussion of this scaling approach including examples demonstrating its applicability for scaling ice-induced vibrations for the Molikpaq platform and Norströmsgrund lighthouse tested during the same campaign can be found in Ref. [20].

For the tests used in this study the scale factor was defined as $\lambda_m = 1700$. This value was obtained using an estimate for the full-scale mean brittle crushing of 1.7 MN and an estimate for the mean brittle crushing load in the basin of 1 kN. The full-scale load was based on a scenario representative of 50-year return period Southern Baltic Sea design conditions ($h_{50} = 0.4$ m, $C_{R,1} = 1$ MPa), which are in line with the data presented in Refs. [22,23], noting that these parameters will vary from site to site. During testing we found that the mean load was actually higher than we had initially estimated, which makes that the experimental results represent a scenario with a higher (≈2.2 MN) mean brittle crushing load.

During the test campaign scaled modal properties of a lumped mass model of an offshore wind turbine were programmed on the micro-controller. Global bending modes up to 20 Hz natural frequency were considered as advised for analysis of dynamic ice-structure interaction in ISO 19906 [24]. Structural frequencies f, critical damping ratios for an idling and operational turbine at rated wind speed ζ and scaled mass-normalized mode shape amplitudes in ice drift direction φ_y and perpendicular to the ice drift direction φ_x are provided in Table 2.

To simulate an operational turbine in the tank we used a pre-defined thrust force F_{wind} applied numerically at the top of the tower in the micro-controller. For this purpose, scaled mass-normalized mode shape amplitudes at tower top were added to the structural model

Table 2
Scaled modal information at ice-structure interaction point and tower top for the structural lumped mass model. Subscripts *idl* and *oper* indicate idling and operational scenarios, respectively. Subscript *MSL* indicates modal amplitudes at Mean Sea Level, and subscript *TT* at Tower Top.

STRUCTURAL MODE	f	ζ_{idl}	ζ_{oper}	$\varphi_{x,MSL}$	$\varphi_{y,MSL}$	$\varphi_{x,TT}$	$\varphi_{y,TT}$
	[Hz]	[%]	[%]	[10^{-3} kg$^{-0.5}$]	[10^{-3} kg$^{-0.5}$]	[10^{-3} kg$^{-0.5}$]	[10^{-3} kg$^{-0.5}$]
1	0.153	0.8	1.0	−1.86	0.00	−39.10	0.00
2	0.154	0.8	10.2	0.00	1.88	0.00	39.39
3	0.824	1.2	1.8	12.66	0.00	52.14	0.00
4	0.888	1.3	4.4	0.00	−14.79	0.00	2.20
5	1.50	2.6	3.4	19.29	0.00	−10.55	0.00
6	1.66	1.9	5.9	0.00	−18.72	0.00	8.14
7	2.72	5.4	5.8	9.49	0.00	13.00	0.00
8	2.91	4.1	5.8	0.00	−7.53	0.00	−13.93
9	5.11	5.4	5.8	−9.39	0.00	−9.24	0.00
10	5.21	5.4	5.8	0.00	−10.04	0.00	−10.44
11	7.46	5.4	5.8	18.60	0.00	−7.25	0.00
12	7.54	5.4	5.8	0.00	18.54	0.00	−8.23
13	10.5	5.4	5.8	−2.35	0.00	−6.83	0.00
14	10.5	5.4	5.8	0.00	−1.95	0.00	−7.66
15	13.4	5.4	5.8	−16.12	0.00	−4.29	0.00
16	13.4	5.4	5.8	0.00	16.08	0.00	4.70
17	15.2	5.4	5.8	0.00	−7.03	0.00	−3.73
18	15.3	5.4	5.8	6.14	0.00	3.43	0.00
19	17.3	5.4	5.8	−9.17	0.00	4.98	0.00
20	17.3	5.4	5.8	0.00	8.70	0.00	−5.51

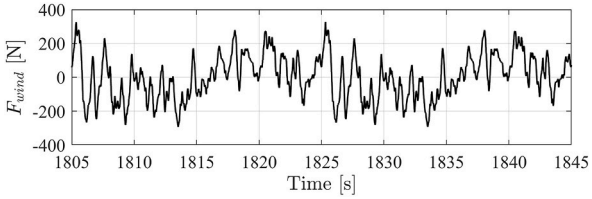

Fig. 2. Applied scaled numerical wind thurst force fluctuations for testing of an operational turbine.

(see Table 2). The thrust force was defined at rated wind speed for the turbine considered and was scaled down with the same factor as the ice load. Before application, the mean wind force was subtracted from the signal to reduce the static offset of the structural setup. Because of limitations with respect to memory, a time series of maximum 2000 data points could be predefined and applied during the tests. As the test durations exceeded the length of the predefined wind force fluctuations, the time series was applied periodically. An example of the applied thrust force, extracted from test ID 624, is shown in Fig. 2. Additionally, linearized aerodynamic damping was added to the structural damping when an operational turbine was simulated (see Table 2).

2.2. Numerical analysis

The numerical simulations in the present study are preliminary simulations performed to obtain insight into the relevance of the experimentally identified regimes of ice-induced vibrations for the design of an offshore wind turbine support structure. For this purpose, a phenomenological ice model from literature, specifically developed for the simulation of dynamic ice-structure interaction, was coupled to a commercial in-house software package (BHawC). BHawC allows to simulate the dynamics of a complete offshore wind turbine and has been used to verify and validate open-source turbine models [25]. The approach chosen allows to provide a realistic estimation of the bending moments that develop over the support structure at the cost of limited reproducibility. It is noted that the ice model is public and input parameters for the simulations are provided below. As BHawC was used for verification and validation of open-source code, the ice model can be coupled to open-source turbine models to obtain qualitatively similar results as presented in this article.

2.2.1. Ice model

The ice model used for this work is defined in detail in Ref. [26], including validation with full-scale data from a lighthouse and model-scale data from several campaigns. It is a phenomenological model which defines the global ice load on a vertically sided structure as a result of interaction with sea ice. The model uses six input parameters which define the ductile and brittle behaviour of the ice and the ice drift speed. Values for these parameters can be determined based on the method described in Ref. [26], which has also been applied to obtain the simulation parameters defined below.

To apply the ice model for simulations with offshore wind turbines, the input parameters need to be defined for the ice conditions concerned. For this purpose, the characteristic peak design load during continuous brittle crushing is obtained based on [24] as:

$$F_G = hwC_R\left[\left(\frac{h}{h_1}\right)^n\left(\frac{w}{h}\right)^m + f_{AR}\right] \tag{1}$$

where F_G is the peak global ice load during continuous brittle crushing, w is the projected width of the structure, h is the ice thickness, h_1 is a reference thickness of 1 m, n and m are empirical coefficients, f_{AR} an empirical term and C_R is the ice strength coefficient. This formula gives a deterministic estimate of the peak brittle crushing load which can be used for design, but not necessarily the true load on the structure in the given scenario.

For the ice model the parameters are chosen such that during continuous brittle crushing the peak load obtained from Eq. (1) has a 50% probability of exceedance in the simulation of a standard crushing event. The standard crushing event is characterized by an ice drift speed and associated crushed length, or penetration depth, corresponding to a stable condition of continuous brittle crushing. This approach is comparable to that used to define the C_R coefficient by Kärnä and Qu [27]. The standard stable brittle crushing event was defined here based on full-scale data as a crushed length of 90 m at an ice speed of 0.15 m s^{-1}.

The input parameters for the simulations as given in Table 3 are then obtained by substitution $h_{50} = 0.4$ m, $C_{R,1} = 1.38$ MPa into Eq. (1) to obtain the target peak brittle crushing load in the standard crushing event. The somewhat high value of $C_{R,1}$ used here, when the Southern Baltic Sea is concerned, is chosen to have the mean load in the numerical simulations equal to the full-scale load corresponding to the the tank experiments for the given scale factor.

Due to its phenomenological nature certain physical effects are likely to not be captured in the model. As indicated in a recent analysis by Gagnon [28], the instantaneous removal of failed ice results in an underprediction of the damping from the ice. This will have to be addressed in a future update of the model. For the purpose of this study the important thing is that the ice model used captures all relevant regimes of ice-induced vibrations as observed in the experiments, which is verified in Section 4.

2.2.2. Wind turbine model

The ice model is fully-coupled to the Bonus Horizontal axis wind turbine Code (BHawC), which is a nonlinear aeroelastic tool for the dynamic analysis of offshore wind turbines developed by Siemens Gamesa Renewable Energy.

Table 3
Ice model input parameters used for numerical analysis.

ICE MODEL PARAMETERS	K_1	K_2	C_1	C_2	N	δ_f	r_{max}
	[N m^{-1}]	[N m^{-1}]	[N m^{-1}s]	[N^3 m^{-1}s]	[−]	[m]	[m]
	$8.52 \bullet 10^6$	$3.26 \bullet 10^7$	$3.06 \bullet 10^7$	$1.11 \bullet 10^{18}$	58	0.004	0.006

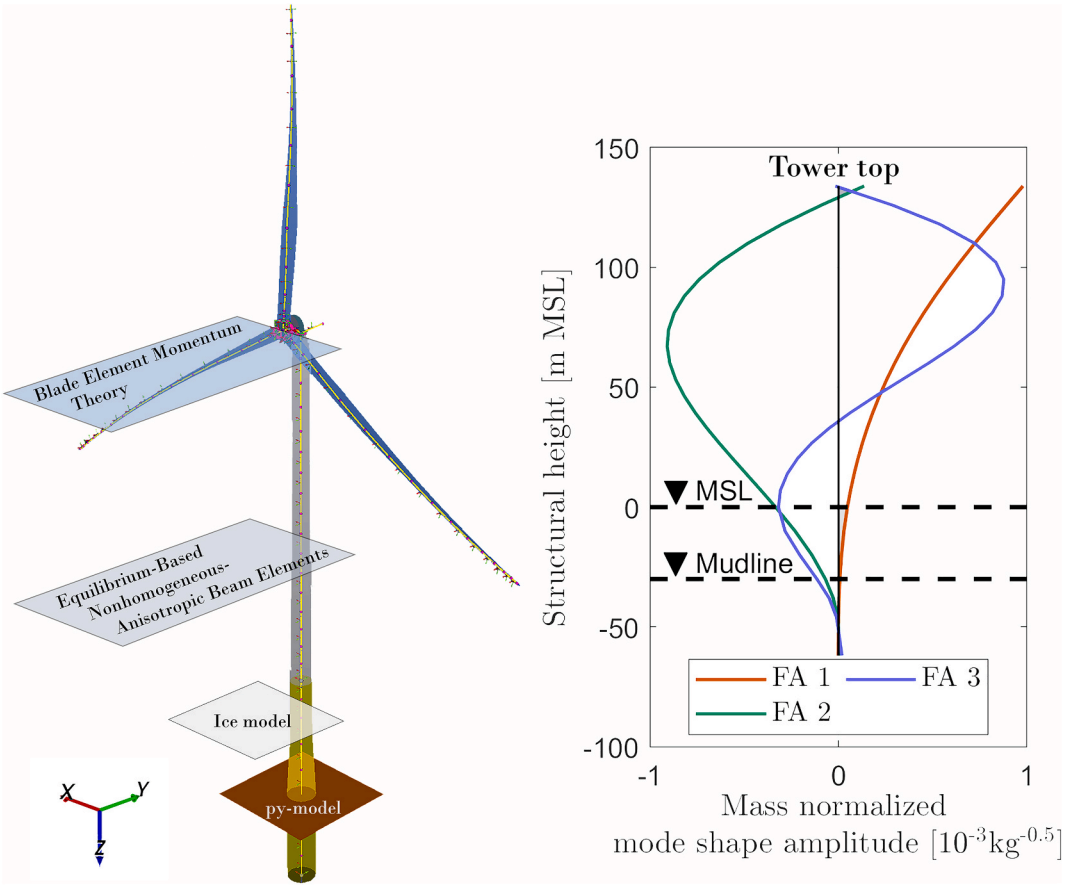

Fig. 3. Left: Wind turbine model. Right: The first three global bending modes of the modelled structure. The fore-aft direction is denoted FA.

BHawC solves substructures for foundation, tower, nacelle, shaft, hub and blades using a co-rotational formulation, allowing for geometric nonlinearity [29]. In more detail the structural model is implemented as a combination of the stiffness matrix and section force recovery formulation [30] and a stiffness proportional damping formulation [31]. Aerodynamics are modelled based on the blade element momentum theory, which has been expanded for skewed and unsteady inflow. Corrections for Prandtl's tip loss and thrust at high induction values are implemented. Aerodynamic forces are based on 3D-corrected coefficients for stationary air foil data and are corrected by a Beddoes-Leishman-type model. Further, tower shadow effects are included and aerodynamics on nacelle and tower are calculated. For further detail on the aerodynamics, reference is made to Ref. [32].

Displaced and contained water as well as marine growth on the support structure are modelled as distributed added mass. A sketch of the wind turbine model and the first three mass-normalized mode shape amplitudes of global bending modes are shown in Fig. 3..

The implemented structural model in this case study is representative of a 14 MW wind turbine on a monopile foundation with a diameter of 7.5 m at mean sea level (MSL). The tower top is roughly 134 m above MSL and the interface between tower and transition piece at 14 m above MSL. The water depth was assumed arbitrarily as 30 m resulting in the pile tip at 62 m below MSL. The structural model consists of 92 Equilibrium-Based Nonhomogeneous Anisotropic Beam Elements resulting in a model with 547 degrees of freedom. The soil is represented by linearized p-y-curves representative for the Baltic Sea. The damping for the foundation and tower were tuned to 5.0 δ % and 8.3 δ % for the first and second global bending mode, respectively (i.e., Rayleigh damping). The model was implemented such that boundary conditions prevent translational and rotational motion in z-direction.

2.2.3. Simulation matrix

The numerical simulation matrix is given in Table 4. As for the experiments, both an operational and idling case are considered. The operational case is representative for design load case (DLC) D3 at rated wind speed in IEC61400-3-1 [11]. The Wind Turbine

Table 4
Information on numerical simulations performed.

TURBINE STATE	REPRESENTATIVE DLC IN IEC61400-3-1 [11]	ICE DRIFT SPEED	WIND SPEED
		[mm s^{-1}] (start:step:end)	[m s^{-1}] (# seeds)
Operational	D3	(2:1:5), (10:2:70), (70:10:150)	12 (6)
Idling	D8	(2:1:5), (10:2:70), (70:10:150)	1 (6)

Generator (WTG) is in normal power production at rated wind speed, with a normal turbulence model (NTM). The idling case is representative for design load case D8 in Ref. [11]. The wind turbine is idling at a wind speed below the cut-in wind speed (i.e. the speed above which the turbine starts to produce power), with an extreme wind model (EWM).

Relevant ice drift speed intervals for the simulations were defined based on the results from the experimental campaign. A simulation duration of 900 s has been chosen to minimize the effect of initial conditions after an initialisation time of 300 s. For all simulations it is assumed that ice drift and wind directions are aligned. Frequency spectra of the numerical data are based on the last 175 s of the data.

3. Experimental results

Results from the tank experiments are presented. First the results from constant deceleration tests are shown which were used to identify the ice drift speeds for which different regimes of ice-induced vibrations developed. Based on these tests several ice drift speeds were selected for constant speed tests to obtain long time series allowing to analyse the vibrations in more detail. Results for the idling and operational turbine are presented side-by-side to show the effect of the simulated wind loading and added aerodynamic damping on the ice-structure interaction.

3.1. Constant deceleration tests

Figs. 4 and 5 show the result for an idling and operational turbine, respectively, during a constant deceleration test reducing the ice drift speed from 80 mm s^{-1} to 0 mm s^{-1} with a deceleration of ≈0.2 mm s^{-2}. As the velocity decreases, the interaction can be clearly seen to change in both the ice load and structural response plots. At high speed (a) the response amplitude of the structural displacement is small in case of idling, and dominated by the wind load in case of operation. As there is no apparent amplification of the ice load, and the structural response is not dominated by any particular mode, the interaction is deemed to be continuous brittle crushing.

In both cases for an ice speed below 50 mm s^{-1} (b) a more amplified second mode response is observed with some higher load peaks indicating interaction between ice and structure. Around 20 mm s^{-1} this interaction changes again showing a saw-tooth like pattern in both the load and response with a clear first mode contribution as seen in the wavelet plot (c). When the speed gets close to zero the ice load increases to the highest magnitude and the period of the observed saw-tooth becomes longer than the first natural period (d). In these ranges of speeds (b) – (d) ice-induced vibration regimes different from continuous brittle crushing are observed. To allow for identification of these regimes long runs with constant speed were performed for which the results are shown in the next section.

3.2. Constant ice drift speed tests

From the deceleration tests a total of eight ice speeds were chosen for long constant speed runs. Here the analysis focusses on several cycles of the observed interaction for the ice speeds of 5 mm s^{-1}, 20 mm s^{-1}, 40 mm s^{-1}, and 70 mm s^{-1}. These time series were illustrative of the four different regimes of ice-induced vibrations encountered during the experiments. The whole time series of the measured structural displacement, ice load, relative velocity and carriage velocity for these runs are included in Appendix A. The square root of power spectral densities (amplitude spectral densities (ASD)) is presented to minimize the influence of initial vibrations on the spectra in the following figures.

3.2.1. Intermittent crushing

For low ice drift speeds (here: 0.005 m s^{-1}) sawtooth displacement patterns and a corresponding load signal are found representative of intermittent crushing (see Fig. 6). The amplitude spectral densities of both global ice load and structural displacement show peaks somewhat below the first linearized natural frequency which are associated with the periodicity of the larger sawtooth observable in the time series. Comparing the operational to the idling case the oscillations in the relative velocities seem to be reduced, which could be related to the higher damping suppressing higher mode oscillations of the structure. The wind load fluctuations do not appear to have a large effect on the overall interaction between the ice and turbine in this regime.

3.2.2. Multi-modal interaction with first mode amplified response

A slightly higher ice drift speed (here: 0.020 m s^{-1}) results in a structural response dominated by an amplified first mode response (see Fig. 7). The global ice load pattern shows a saw-tooth like shape; however, the main periodicity is closer to the first natural period of the structure when compared to Fig. 6. The regime does not fall within the definitions for ice-induced vibrations adopted in

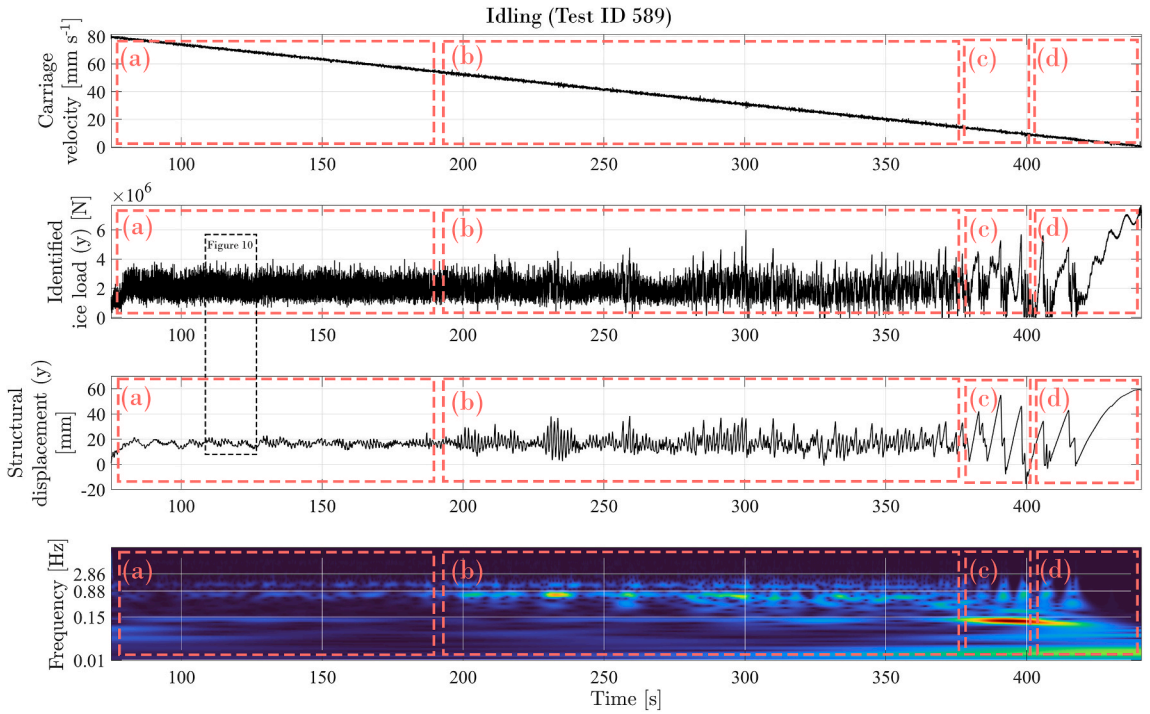

Fig. 4. Results from a constant deceleration test for an idling wind turbine. From top to bottom: Low-pass filtered carriage velocity, identified ice load, structural displacement at the ice action point, wavelet plot of the structural displacement indicating the frequencies of the first three eigen modes on the ordinate axis. Different regimes of ice-induced vibrations are approximately indicated with (a) to (d).

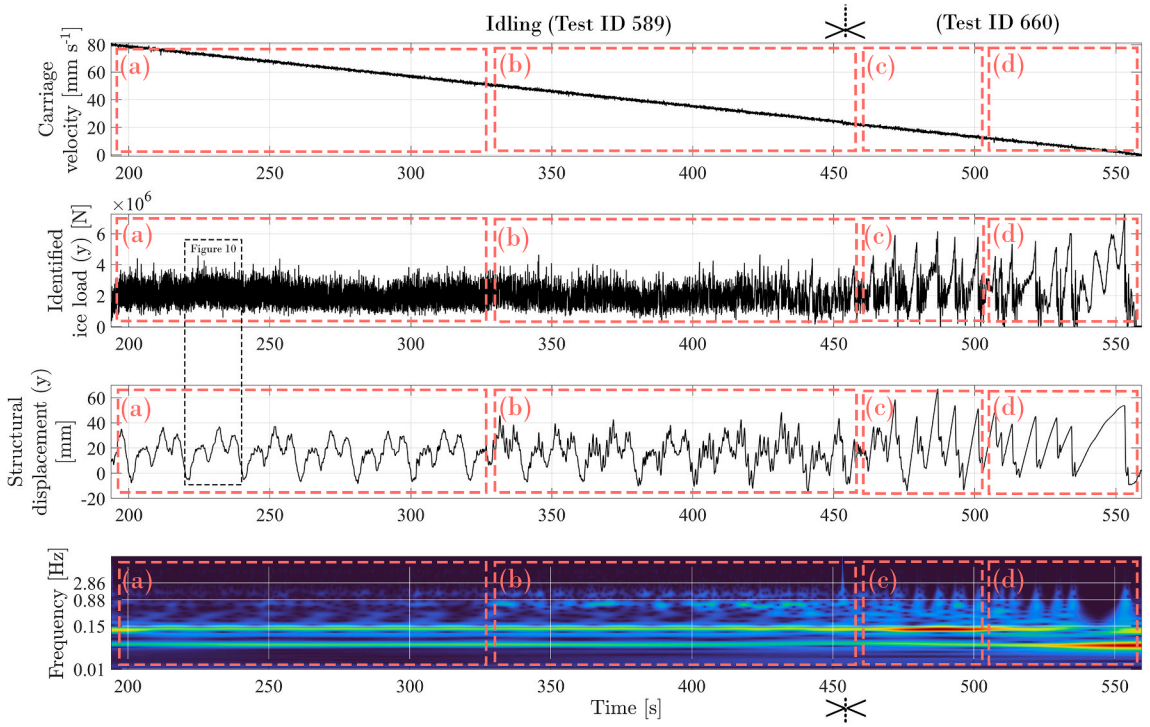

Fig. 5. Results from a constant deceleration test for an operational wind turbine. From top to bottom: Low-pass filtered carriage velocity, identified ice load, structural displacement at the ice action point, wavelet plot of the structural displacement indicating the frequencies of the first three eigen modes on the ordinate axis. Different regimes of ice-induced vibrations are approximately indicated with (a) to (d).

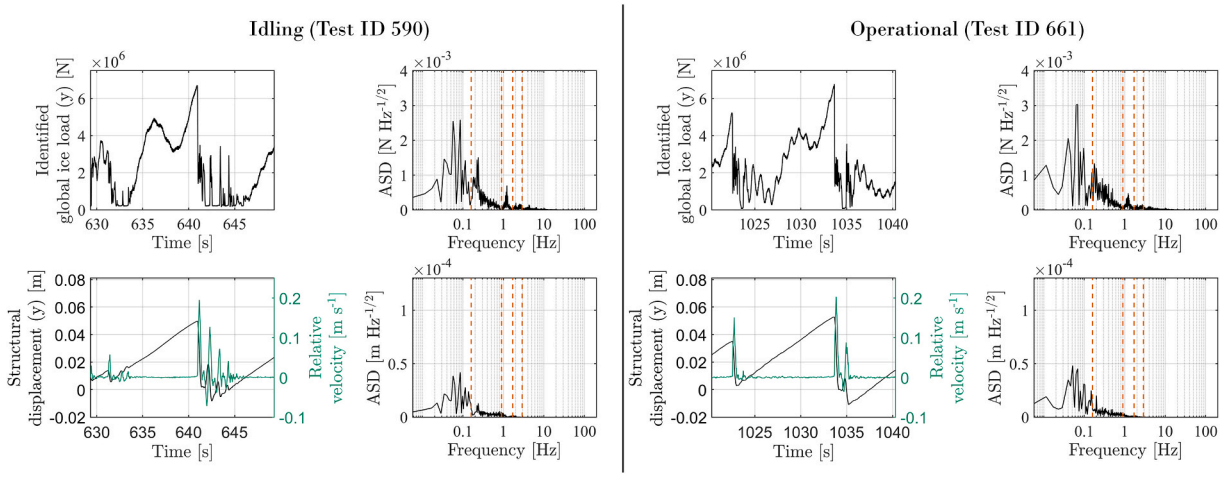

Fig. 6. Time series of ice load, structural displacement and relative velocity and amplitude spectral densities of ice load and structural displacement of an idling (left) and operational (right) turbine for a constant ice drift speed test (here: 0.005 m s^{-1}).

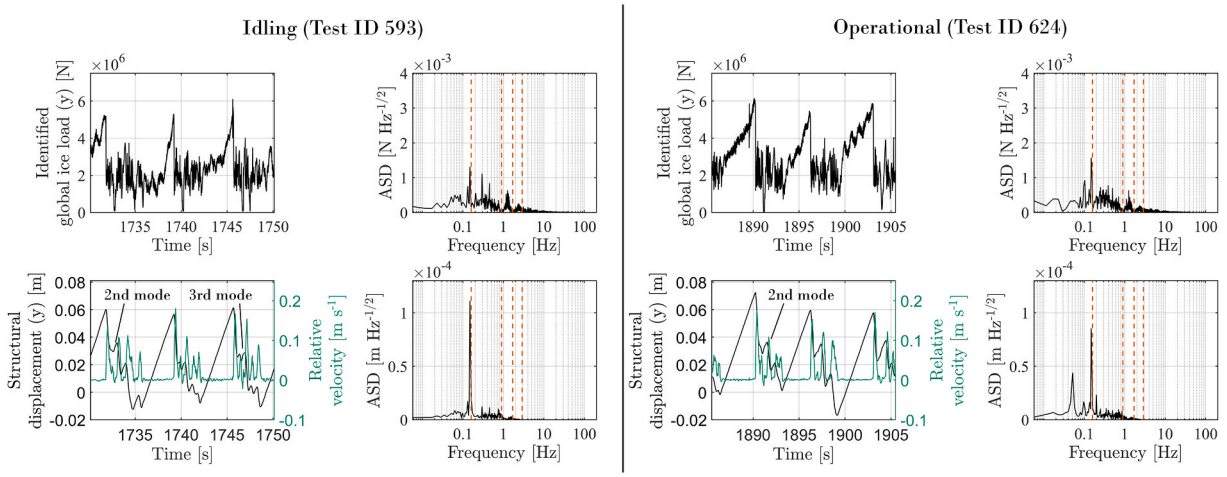

Fig. 7. Times eries of ice load, structural displacement and relative velocity and amplitude spectral densities of ice load and structural displacement of an idling and operational turbine for a constant ice drift speed test (here: 0.020 m s^{-1}).

ISO19906 and IEC61400 and literature [33]. The response of the structure is not dominated by a harmonic response in a single mode, which would characterize it as frequency lock-in. Instead, the second and third mode of the turbine get involved once the structure moves back to its origin after an event of global ice failure. The possibility for multi-modal ice-induced vibrations to develop has been observed during experiments conducted by Määttänen [34], though not in a situation with a controlled indentation speed.

The short period of second-mode vibration may develop because the first mode is relatively slow. When the structure returns to the equilibrium after large global ice failure the oscillations in relative velocity indicate short instances of frequency lock-in in the second mode to develop. As there is enough time during half a period of first mode vibration (≈3 s) for several cycles of second mode oscillation to develop, and the second mode of the turbine can be easily excited by the ice (see Fig. 3), it is made impossible for 'classical' frequency lock-in to develop for the first mode. In a way, the motions in the second mode, and to some extent the third mode, act as a disturbance.

Comparing the results for the idling and operational turbine, no clear differences are observed except for the peak in the ASD plot of the structural displacement at a frequency of 0.05 Hz which relates to the imposed fluctuating wind load.

3.2.3. Frequency lock-in

For intermediate ice drift speeds in the experiment (here: 0.040 m s^{-1}) a near-harmonic oscillation with a frequency slightly below the second natural frequency of the structure is found, which classifies as frequency lock-in (see Fig. 8). Some short moments of third

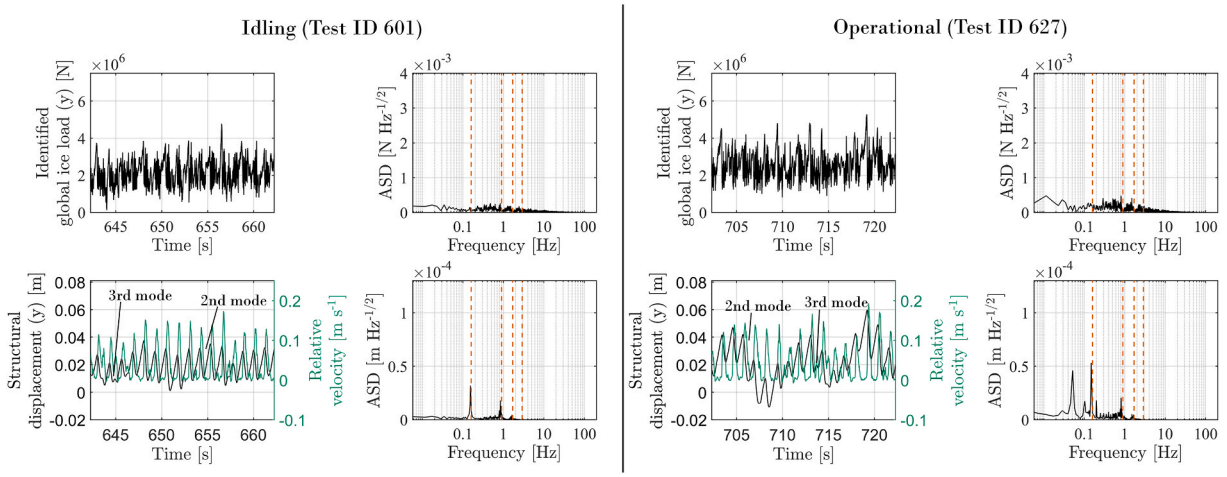

Fig. 8. Timeseries of ice load, structural displacement and relative velocity and amplitude spectral densities of ice load and structural displacement of an idling and operational turbine for a constant ice drift speed test (here: 0.040 m s^{-1}).

mode interaction can be seen to develop for low relative velocities (around minima of the displacement signal). The global ice load is periodic, but with smaller peak load amplitudes than observed for the lower speeds. For this type of interaction, the wind induced response is clearly visible in the displacement signal during the operational case. The effect on the ice load and relative velocity between ice and structure seem to be minimal.

For confirmation of the qualification as frequency lock-in, we show the structural peak velocities in the direction of the ice motion v_{peak} for all tested ice drift speeds v_{ice} in Fig. 9. A linear relation between these two parameters (β) can be used to identify frequency lock-in [35]:

$$v_{peak} = \beta v_{ice} \tag{2}$$

with β between 1.0 and 1.5. The peak velocity was calculated for the 99th quantile of the last half of the timeseries to exclude outliers. Based on the plot, frequency lock-in occurs for an ice drift speed between 0.020 and 0.050 m s^{-1}. However, the time series clearly indicate that the structure experiences a different type of vibration pattern for an ice drift speed of 0.020 m s^{-1}. As the method is based on single-degree of freedom structures, this method might be insufficient when applied for multi-degree of freedom structures, though it still gives a reasonable indication of where (temporary) lock-in might have developed. The differences of the structural peak velocity between the idling and operational scenarios can be explained by the difference in aerodynamic damping. An ice drift speed between 0.005 and 0.020 m s^{-1} causes ice-induced vibrations with a frequency close to a frequency of the first eigenmode. As the aerodynamic damping is highest for this eigenmode, vibrations are significantly damped. Differences for higher ice drift speeds are marginal as the effect of aerodynamic damping on the structural peak velocity reduces due to a different type of structural response.

The amplitude spectral density of the structural displacement in Fig. 8 shows a contribution of the first mode during frequency lock-in. This is explained by the experiments not lasting long enough for the effects due to initial conditions to diminish.

3.2.4. Continuous brittle crushing

For the highest ice drift speeds included in the experiments no significant structural vibrations and a characteristic stochastic load around a mean level are obtained (see Fig. 10). For an operational turbine, the numerically applied wind load fluctuations at tower top can be recognized in the structural response at the ice action point. Neither the idling nor the operational ice load spectrum indicates any specific ice breaking frequency in this regime.

4. Numerical qualification of importance of different IIV regimes for design

The experimental results presented in Section 3 do not reveal the effect of the ice-induced vibrations on the full support structure of the turbine, but rather only at the ice action point. Preliminary numerical simulations were performed to gain some insight in the relative importance of the observed regimes of ice-induced vibrations for design of a support structure. The results of these simulations are presented here. First, the ability of the adopted phenomenological ice model to qualitatively capture the different regimes of ice-induced vibrations observed in the experiments is verified. This is followed by the presentation of the maximum absolute bending moments over the height of the support structure for different ice speeds. These bending moment plots are used to identify the relative importance of the different ice-induced vibration regimes for design.

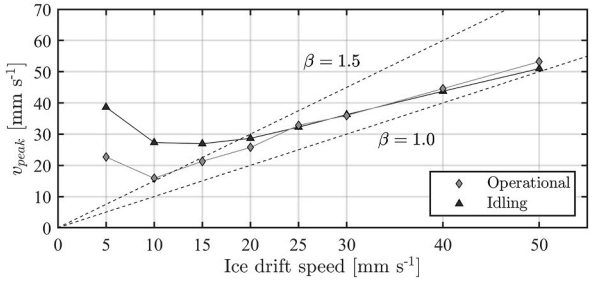

Fig. 9. Structural peak velocities in the direction of ice motion are presented for eight tested constant ice drift speeds.

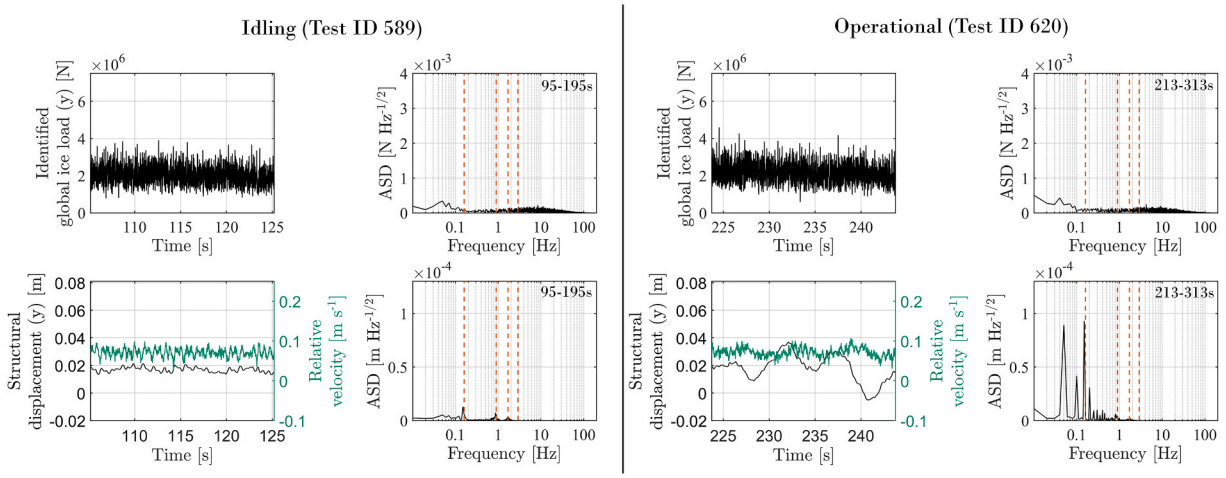

Fig. 10. Time series of ice load, structural displacement and relative velocity and amplitude spectral densities of ice load and structural displacement of an idling and operational turbine for a quasi-constant ice drift speed test (here: 0.070 m s^{-1}).

4.1. Numerically obtained ice-induced vibration regimes

Figs. 11 and 12 provide an overview of the numerically obtained ice-induced vibration regimes for different ice speeds in the same format as Figs. 6–8 and 10, for an idling and operational turbine, respectively. For an idling turbine all four experimentally identified regimes of ice-induced vibrations were found in the numerical simulations. Intermittent crushing developed for an ice speed of 5 mm s^{-1}. An example of amplified first mode response has been selected for an ice speed of 38 mm s^{-1}. An example of frequency lock-in in the second mode is shown for an ice speed of 48 mm s^{-1} and at higher speeds (e.g., 150 mm s^{-1}) the simulation resulted in continuous brittle crushing. For the operational turbine similar results were obtained, with the effect of wind loading clearly visible for the higher ice speeds simulated. A difference between the numerical and experimental results for the operational turbine is the mean offset of the displacement, which was not included in the experiments to avoid having to offset the actuators.

Qualitatively the results match the experimental observations well allowing to use the results to assess the relative importance of the regimes of ice-induced vibrations for design. We note that the numerical model results in more regular load and displacement patterns as the model assumes perfectly homogeneous ice, whereas real ice and the ice in the tank are characterized as an inhomogeneous material with both thickness and strength varying across the sheet.

4.2. Bending moments along the support structure

The maximum bending moments over the height of the support structure are presented in Fig. 13. These are the maxima from six simulations with different wind seeds for the idling and operational cases as introduced in Table 4. Local maxima per cross-section are indicated in purple. It is found that regardless of operation or idling, the maximum bending moments per cross-section occur when the

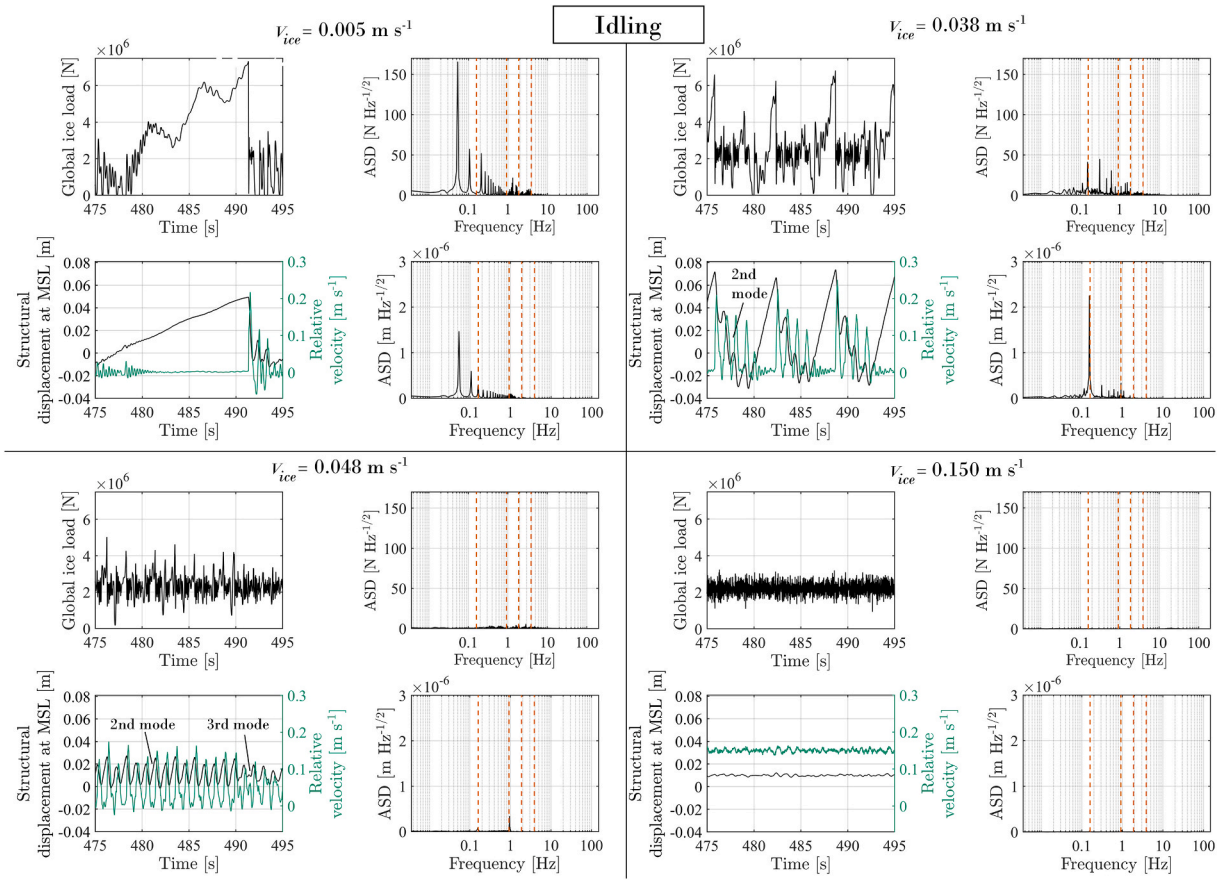

Fig. 11. Characteristics of global ice load and structural displacement at MSL for four representative ice drift speeds for an idling turbine. For each ice drift speed four plots represent the ice load time series (top left), amplitude spectral density of the ice loads (top right), structural displacement time series (bottom left) and amplitude spectral density of structural displacement (bottom right). Dashed orange lines mark the frequencies of the first four structural eigenmodes.

ice drift speeds are low, in the range of 0.002 m s^{-1} up to 0.04 m s^{-1} approximately. These ice drift speeds correspond to the regimes of intermittent crushing and the regime with an amplified non-harmonic first mode response as can be seen in Figs. 11 and 12. The effect of the wind load is clearly seen in the results, as bending moments over the height of the support structure are much larger for the operational scenario when compared to the idling scenario.

5. Discussion

The discussion focusses on the observed regimes of ice-induced vibrations, generalization of the results, and limitations of the experiments.

5.1. Ice-induced vibrations of offshore wind turbines

For the most part the vibrations observed in the experiments for offshore wind turbines are similar to those observed for existing structures in the past. Intermittent crushing develops at low ice drift speeds, frequency lock-in at intermediate speeds, and continuous brittle crushing at high speeds. The results from the constant deceleration tests show transitions from one regime to the other which are comparable to the early observations on slender piles in Cook Inlet by Blenkarn [3], and for example the Molikpaq May 12th event [5]. As offshore wind turbines are relatively compliant structures, it is understandable that these will show severe ice-induced vibrations in much milder ice conditions when compared to, for example, the Molikpaq.

There are two clear differences when comparing the wind turbine results to observations for other types of structures: 1) a multi-modal type of interaction leading to a non-harmonic amplified first mode response develops in between intermittent crushing and frequency lock-in, and 2) frequency lock-in develops mainly in the second global bending mode rather than the first.

The multi-modal type of interaction is shown in Fig. 7 and develops for both an idling and operational turbine. The response is

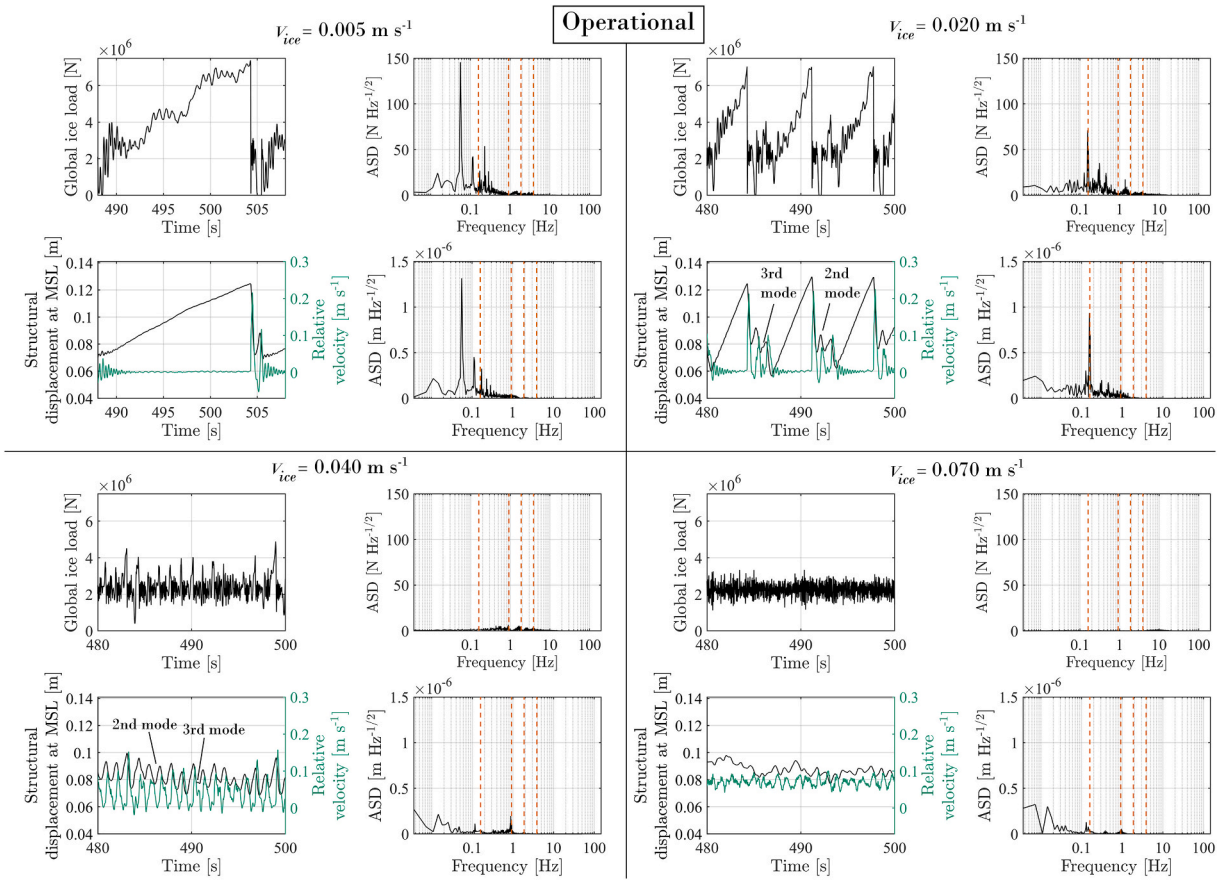

Fig. 12. Characteristics of global ice load and structural displacement at MSL for four representative ice drift speeds for an operational turbine. For each ice drift speed four plots represent the ice load time series (top left), amplitude spectral density of the ice loads (top right), structural displacement time series (bottom left) and amplitude spectral density of structural displacement (bottom right). Dashed orange lines mark the frequencies of the first four structural eigenmodes.

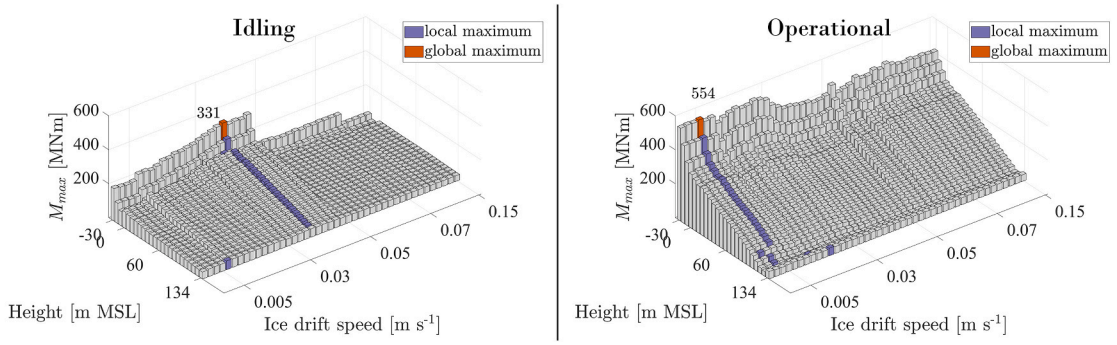

Fig. 13. Maximum bending moment over the height of the support structure for different design load cases and simulated ice drift speeds.

characterized by a main period roughly equal to the first natural period of the structure, with contributions of the second and third mode during half the cycle when the main direction of motion of the structure is towards the ice. The response of the structure not being harmonic, makes this interaction not fit with the definition of frequency lock-in. The interaction not being quasi-static makes it not fit with the classical definition of intermittent crushing. This regime is perhaps best qualified as 'something in between'. The occurrence of this regime can be explained based on the particular modal properties of an offshore wind turbine.

It is generally known that the periodicity in the ice load and structural response, provided ice-induced vibrations develop, decreases

with increasing ice drift speed. Once the periodicity gets close to that of one of the structural modes, the interaction may change from intermittent crushing into frequency lock-in. This only happens when the structural mode is lightly damped, the frequency is relatively low (<10 Hz is a commonly used threshold [24]) and the mode can be easily excited by the ice. For lighthouses and channel markers only the first mode typically fulfils these criteria, resulting in lock-in in the first mode only when the ice conditions are severe enough. For offshore wind turbines the first mode fulfils these criteria, but the second and third mode do as well. Fig. 3 shows the mass-normalized modal amplitudes for the wind turbine studied in the present study, where it can be clearly seen that at the location of the ice action point (i.e at MSL) the second and third global bending mode can be easily excited.

In a scenario where the constant ice drift speed reaches the range where frequency lock-in in the first mode could theoretically develop for the wind turbine, the response amplitude is amplified. The global ice load also shows a main periodicity equal to that of the first mode. After a moment of global ice failure though, the structure starts to move towards the ice increasing the relative velocity between ice and structure. As the first mode is relatively slow, this relative velocity does not change very rapidly. When the relative velocity becomes higher than the incident ice drift speed the conditions for lock-in in the second or third global bending mode are created. As these modes have significantly shorter periods than the first mode, and low damping, the interaction develops quickly and for a couple of cycles. This 'lock-in' with the second or third mode disturbs the development of a quasi-harmonic first mode response of the structure causing the response pattern to look different from what is typically observed in frequency lock-in.

For frequency lock-in in the second mode, developing at higher ice speeds, this interference effect of higher modes is much more limited. We still saw some third mode oscillations, but in general the response was much closer to harmonic as known for other structures.

The numerical simulations show the relevance of the different regimes of ice-induced vibrations for design. When the ultimate limit state is concerned these are intermittent crushing and the newly identified regime that result in the largest bending moments of the structure. For fatigue analysis the frequency lock-in could be important as well, though this depends on the specific probabilities associated with different ice drift speeds. It is noted that the low ice drift speeds do not need to be constant for a long time to lead to individual high load and response peaks, as can be seen from the constant deceleration tests in Figs. 4 and 5.

5.2. Generalization of results

The results presented are specific to the case considered in this study in terms of absolute numbers for both the experiments and the numerical simulations. Qualitatively though, these can be generalized for monopile support structures of offshore wind turbines. Most support structures for offshore wind turbines have the second or third global bending mode excited easily at the ice action point, and therefore the interaction can be expected to develop as observed in the experiments. For larger turbines the third mode influence is likely to become more significant as the peak of the mode shapes shift with respect to each other with the height of the support structure. For smaller turbines, such as those currently installed in the Baltic Sea, it will mainly be the second global bending mode. Regardless of the modes involved in the interaction, these will always be the low ice speeds which will result in the largest structural response and are considered most relevant for design of a support structure.

In terms of ice conditions, it is more challenging to generalize the results, though for more severe ice conditions than those scaled in the tank the boundaries between different interaction regimes will theoretically shift to higher ice drift speeds and vice versa [36].

5.3. Limitations of the study

In our experiments we did not observe buckling failure as seen in earlier tests [12,13], owing to the relatively high flexural strength of the cold model ice. The introduction of this new type of model ice during the campaign did come with challenges as we do not have an accurate estimation of the compressive strength due to the measurement system not being able to deal with the high strength forcing the ice sample to fail in bending rather than compression. This needs to be resolved in future experiments.

The initial impact between the ice and the structure at the start of a test would often result in excitation of the first mode. This transient effect took a lot of time to disappear owing to the long natural period and low damping. As a consequence, there was often not enough test length in the tank during high-speed tests to reach a state where the first mode was no longer visible in the response of the structure. Though in reality such effects would also occur when ice first impacts a turbine support structure, the analysis of the results in the frequency domain is somewhat complicated by this as it cannot be confirmed if the first mode contribution is just transient or really part of the steady-state response. To reduce the effect of initial vibrations on the spectrum analysis, amplitude spectral densities instead of power spectral densities have been shown.

A challenge with tank testing for ice crushing in general is how to deal with scaling. To verify that our experiments result in representative load and response patterns for full-scale we have included tests with a simulated Molikpaq platform and Norströmsgrund lighthouse in the test campaign. These structures are amongst the most well-known real structures which have experienced ice-induced vibrations in full-scale while measurement campaigns were conducted. The results of these tests are reported upon in Ref. [20]. The experiments for the Molikpaq reproduced the development of intermittent crushing like observed in the famous May 12th' 1986 event [37], and for the Norströmsgrund lighthouse only short periods of lock-in developed representative of those during three winters of measurements [38]. Given these results for the existing structures we are confident that the experimental results for

the offshore wind turbine are representative of full-scale interaction.

This study did not investigate particularly how structural properties, non-linear effects, soil or passive dampers, and rotor-nacelle-assembly related aspects such as blade pitch angles, yaw errors and blade passing influence the ice-structure interaction development. Inclusion of such effects in the experiments is theoretically possible with the hybrid test setup but was omitted as it was expected that the inclusion of such effects would significantly complicate the interpretation of the results.

At the time of development of this work the IEA 15 MW turbine model [39] was not available yet. That turbine model can be used in simulations to verify the results of this study in terms of effects of wind loading on the interaction with the ice and to further investigate effects of ice loading on the rotor-nacelle-assembly in general. As BHawC was used for validation of the open-source code FAST [25], results of this study can be reproduced provided the ice model used in this study is coupled to FAST.

6. Conclusion

Ice basin tests for offshore wind turbines with a monopile foundation in ice conditions representative of severe Southern Baltic Sea conditions have shown the development of all known regimes of ice-induced vibrations and in addition a multi-modal type of interaction regime. This multi-modal interaction developed for both an idling and operational turbine at ice speeds between those for which quasi-static intermittent crushing and frequency lock-in in the second global bending mode were observed. The interaction is characterized by an amplified, non-harmonic, first mode response with contributions of the second and third mode of the turbine after instances of global ice failure.

From the experiments the effect of the wind load fluctuations during operation on the interaction between ice and structure seemed to be minimal, when compared to an idling scenario. The relative contributions of different modes to the structural response changes due to higher aerodynamic damping, but all regimes of ice-induced vibrations showed to develop for both scenarios. For a high ice drift speed, the structural response at the ice action point during operation reflects the wind load fluctuations, whereas at low speeds when severe ice-induced vibrations develop the response shows to be controlled by the ice.

Preliminary numerical simulations have shown that for the full support structure the interaction at low speed resulting in intermittent crushing and the multi-modal interaction regime give rise to the largest bending moments, illustrating the relevance of these regimes of ice-induced vibration for design.

Funding

This work was supported by TKI-Energy by the 'Toeslag voor Topconsortia voor Kennis en Innovatie (TKI's)' of the Dutch Ministry of Economic Affairs and Climate Policy. (grant reference: TKITOE_WOZ_1906_TUD_SHIVER).

Declaration of competing interest

The authors declare that they have no known competing financial interests or personal relationships that could have appeared to influence the work reported in this paper.

Data availability

The raw experimental data can be obtained from the 4TUResearchData respository (https://doi.org/10.4121/17087462.v1). Data of numerical results are not public.

Acknowledgements

The authors thank the participating organizations in the SHIVER project: TU Delft and Siemens Gamesa Renewable Energy for supporting this work. The SHIVER project is co-financed by Siemens Gamesa Renewable Energy and TKI-Energy by the 'Toeslag voor Topconsortia voor Kennis en Innovatie (TKI's)' of the Dutch Ministry of Economic Affairs and Climate Policy.

We thank Dr. Sebastian Schafhirt for his contribution in discussions on damping, Dr. Axel Nernheim for his contribution on soil conditions, Erik Smid for his contribution of foundation and tower design, Bart van den Akker for helpful comments, and both Cody Owen and Dr. Marnix van den Berg for their contribution during the test campaign. We further thank Dr. Marc Seidel for discussions on the test setup and the ice tank team from Aalto university for their remarkable commitment during the test campaign.

Appendix A

Figs. 1–6 below provide the identified ice load, structural displacement, relative velocity and carriage velocity for the long test runs conducted in the study. In the figures the parts of the time series analysed in the main text are indicated.

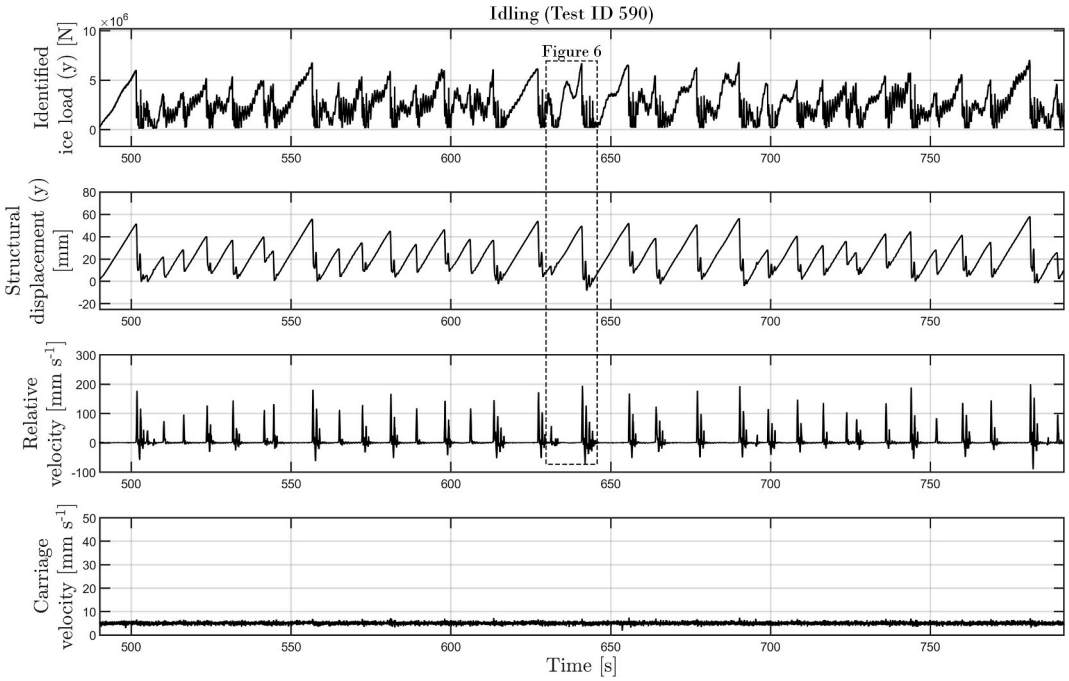

Fig. 1. Experimental results from Test ID 590 at 5 mm s^{-1} (idling).

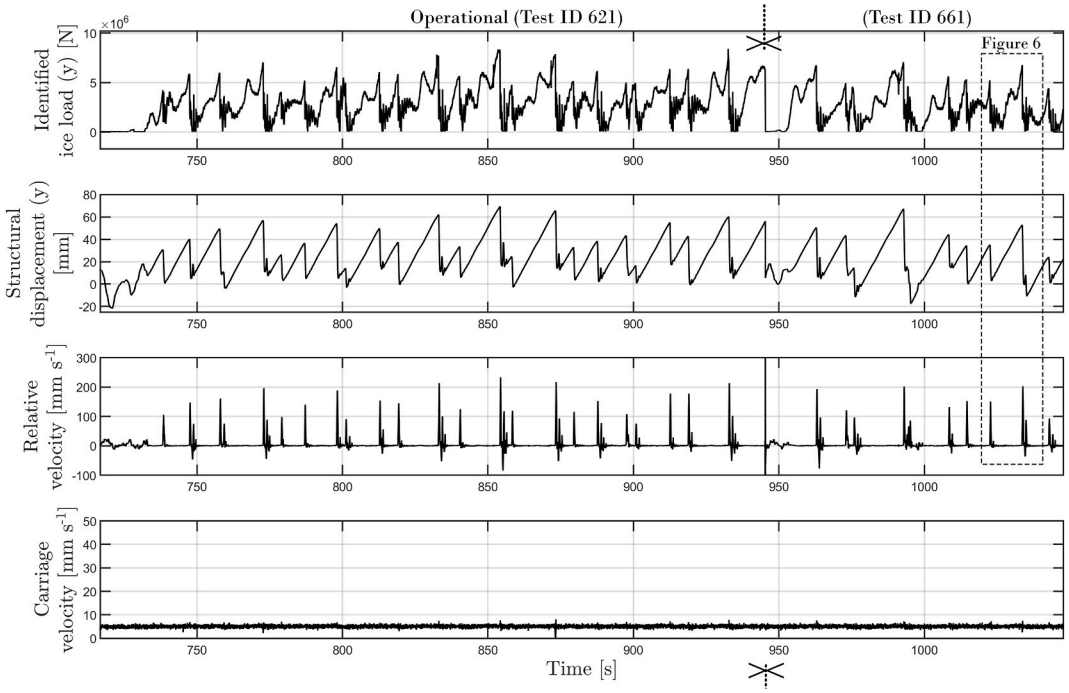

Fig. 2. Experimental results from Test ID 621 and 661 at 5 mm s^{-1} (operational).

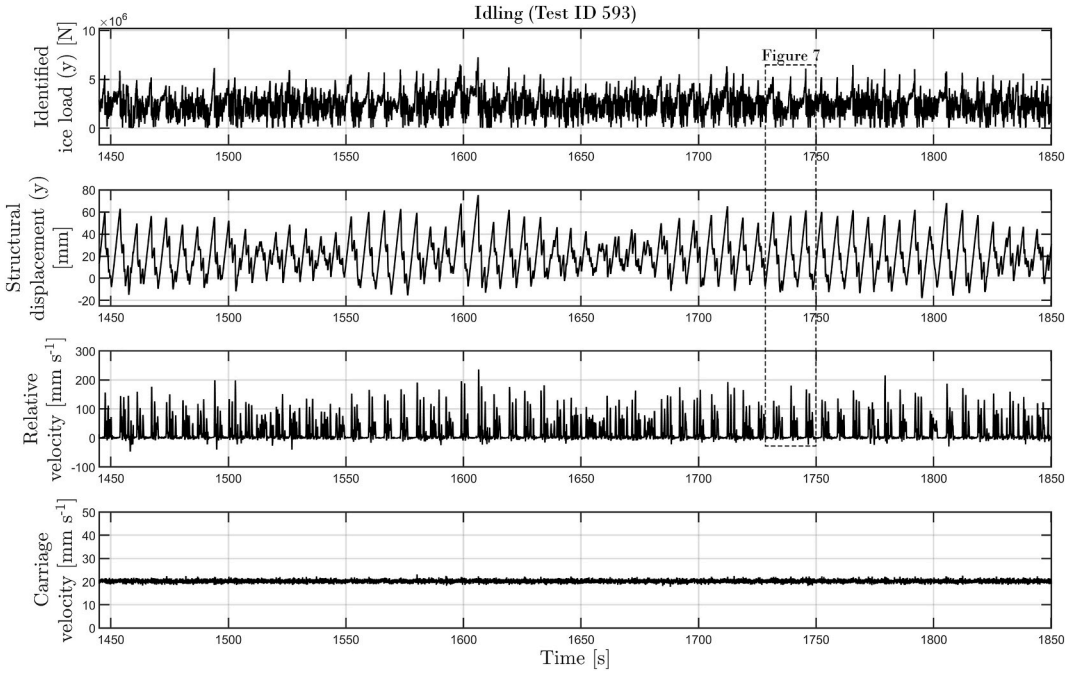

Fig. 3. Experimental results from Test ID 593 at 20 mm s^{-1} (idling).

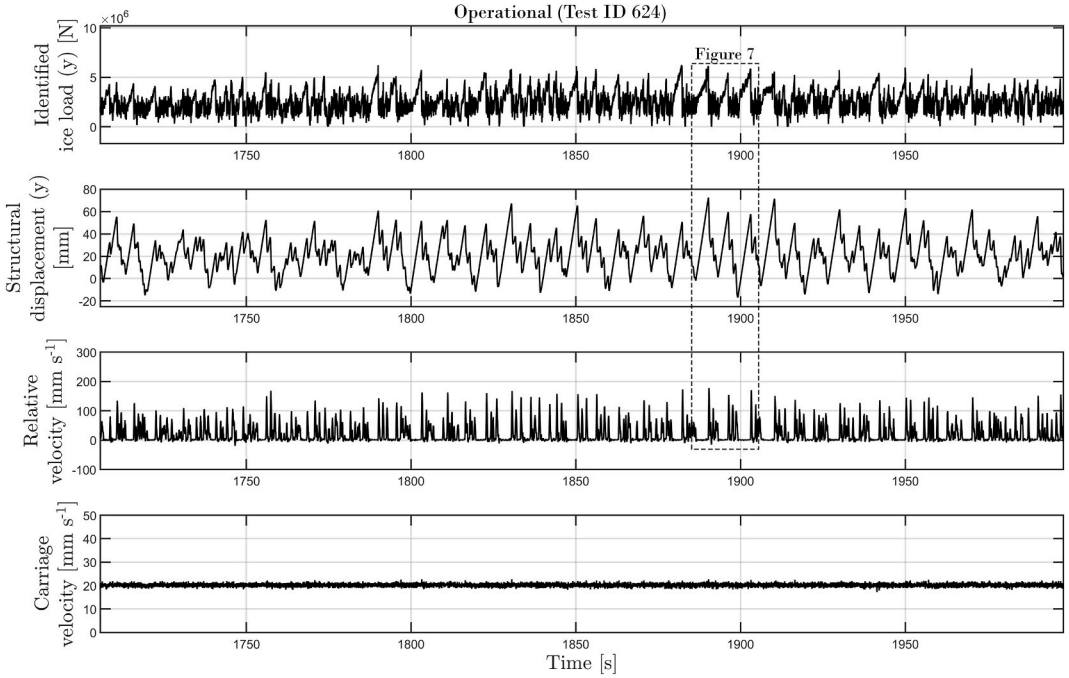

Fig. 4. Experimental results from Test ID 624 at 20 mm s^{-1} (operational).

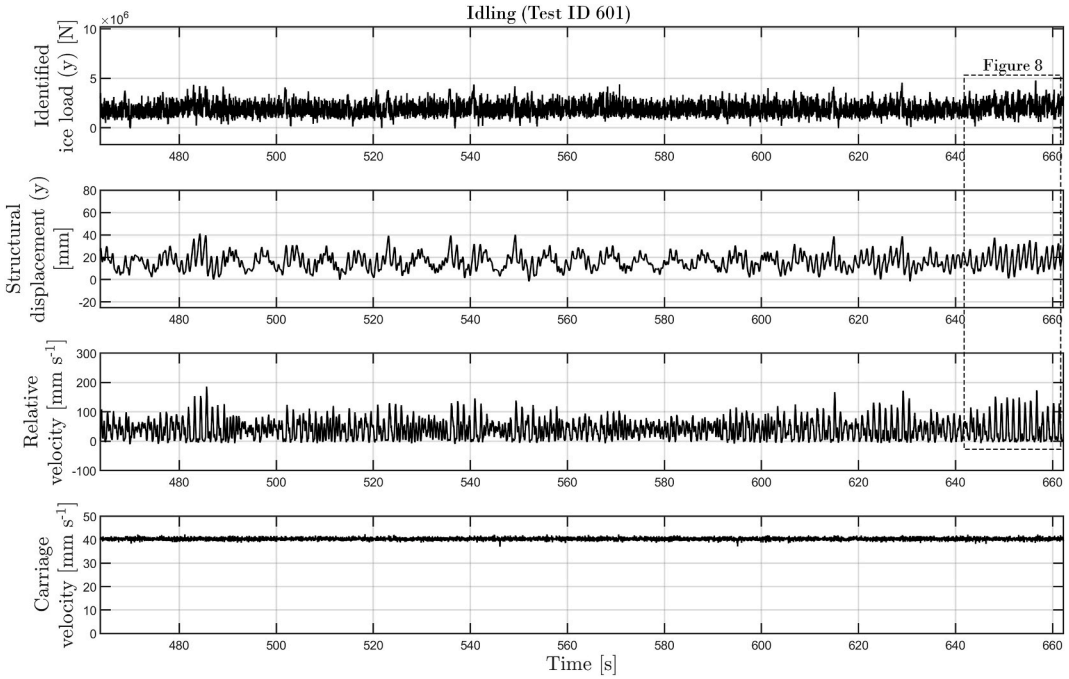

Fig. 5. Experimental results from Test ID 601 at 40 mm s^{-1} (idling).

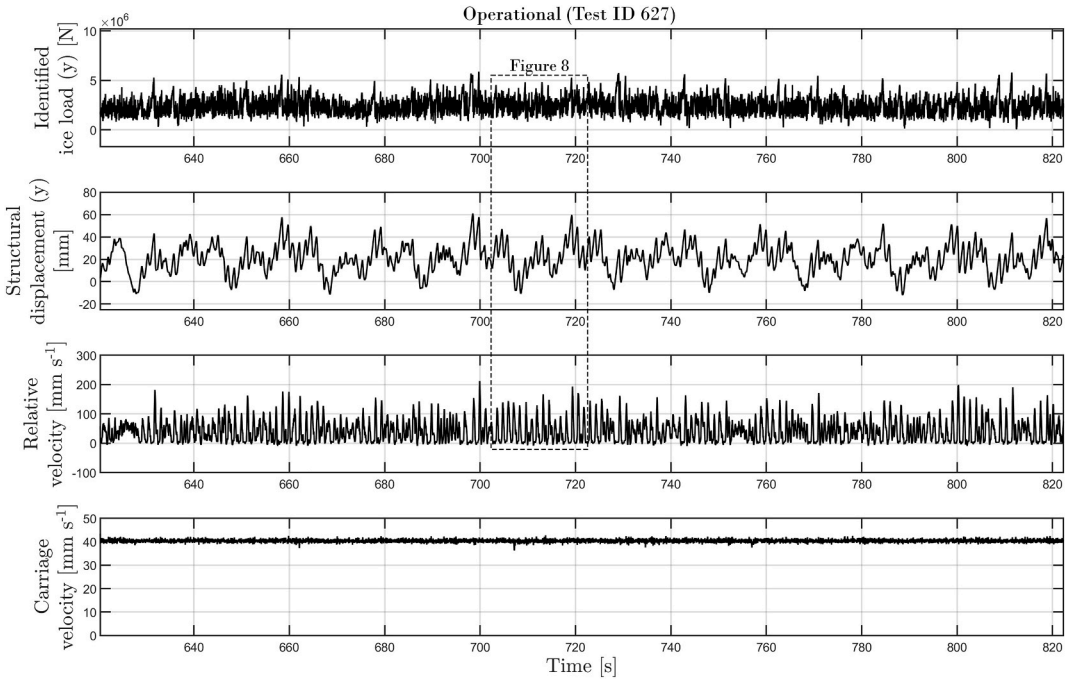

Fig. 6. Experimental results from Test ID 627 at 40 mm s^{-1} (operational).

References

[1] WindEurope. Boosting offshore wind energy in the Baltic Sea. 2019.
[2] Peyton HR. Sea ice forces. Proc. Conf. Ice Press. Against Struct.; 1968. p. 117–23. https://doi.org/10.4224/40001154.
[3] Blenkarn KA. Measurement and analysis of ice forces on cook inlet structures. Proc Annu Offshore Technol Conf 1970;II:365–78. https://doi.org/10.4043/1261-ms.

[4] Yue Q, Bi X. Ice-induced jacket structure vibrations in Bohai Sea. J Cold Reg Eng 2000;14:81–92. https://doi.org/10.1061/(ASCE)0887-381X(2000)14:2(81).
[5] Jefferies MG, Wright WH. Dynamic response of "Molikpaq" to ice-structure interaction. In: Proc. 7th Int. Conf. offshore mech. arct. Eng., vol. IV; 1988. p. 201–20.
[6] Määttänen M. Experience of ice forces against a steel lighthouse mounted on the seabed and proposed construction refinements. In: Proc. 3rd Int. Conf. Port Ocean Eng. under Arct. Cond., fairbanks, Alaska, USA; 1975. p. 857–69.
[7] Engelbrektson A. Dynamic ice loads on a lighthouse structure. In: Proc. 4th Int. Conf. Port Ocean Eng. under Arct. Cond., st. John's, newfoundland, Canada; 1977. p. 654–63.
[8] Nordlund OP, Kärnä T, Järvinen E. Measurements of ice-induced vibrations of channel markers. In: Proc. 9th IAHR int. Symp. Ice, vol. I. Japan: Sapporo; 1988. p. 537–48.
[9] Kamesaki K, Yamauchi Y, Kärnä T. Ice force as a function of structural compliance. In: Proc. 13th IAHR int. Symp. Ice, vol. I. Beijing, China: IAHR; 1996. p. 395–402.
[10] Gravesen H, Kärnä T. Ice loads for offshore wind turbines in southern Baltic Sea. Proc. 20th Int. Conf. Port Ocean Eng. under Arct. Cond. Sweden: Luleå; 2009. p. 12.
[11] International Electrotechnical Commission. Wind energy generation systems. 2019;April. IEC 61400-3-1.
[12] Barker A, Timco GW, Gravesen H, Vølund P. Ice loading on Danish wind turbines. Part 1: dynamic model tests. Cold Reg Sci Technol 2005;41:23p. https://doi.org/10.1016/j.coldregions.2004.05.002.
[13] Hendrikse H, Ziemer G, Owen CC. Experimental validation of a model for prediction of dynamic ice-structure interaction. Cold Reg Sci Technol 2018;151:345–58. https://doi.org/10.1016/j.coldregions.2018.04.003.
[14] Ji S, Yang D. Ice loads and ice-induced vibrations of offshore wind turbine based on coupled DEM-FEM simulations. Ocean Eng 2021:15p. https://doi.org/10.1016/j.oceaneng.2021.110197.
[15] Tian Y, Huang Y, Li W. Experimental investigations on ice induced vibrations of a monopile-type offshore wind turbine in Bohai sea. Proc. 29th Int. Ocean Polar Eng. Conf. 2019:327–34.
[16] Hendrikse H, Hammer TC, Van Den Berg M, Willems T, Owen CC, van Beek K, et al. Experimental data from ice basin tests with vertically sided cylindrical structures. Data Brief 2022;41:18p. https://doi.org/10.1016/j.dib.2022.107877.
[17] Hendrikse H, Hammer T, van den Berg M, Willems T, Owen C, van Beek K. Data from ice tank tests with vertically sided structures collected during the SHIVER project. 4TUResearchData Dataset 2021. https://doi.org/10.4121/17087462.v1.
[18] Hammer TC, Beek K Van, Koning J, Hendrikse H. A 2D test setup for scaled real-time hybrid tests of dynamic ice- structure interaction. In: Proc. 26th Int. Conf. Port Ocean Eng. under Arct. Cond.; 2021. p. 13.
[19] ITTC. Recommended procedures and guidelines. Test Methods for Model Ice Properties; 2014.
[20] Hendrikse H, Hammer TC, Owen CC, Puolakka O, Willems T. Ice basin tests for ice-induced vibrations of offshore structures in the SHIVER project. In: Proc. ASME 2022 41st Int. Conf. Ocean Offshore Arct. Eng.; 2022. https://doi.org/10.1115/OMAE2022-78507.
[21] Ziemer G. Ice-induced vibrations of vertical structures. Tech Univ Hambg (Doctoral Thesis) 2021:170. https://doi.org/10.15480/882.4018.
[22] Willems T, Hendrikse H. Coupled simulation of ice-structure interaction of offshore wind turbines in BHawC using VANILLA. In: Proc. 25th Int. Conf. Port Ocean Eng. under Arct. Cond.; 2019. p. 10.
[23] Tikanmäki M, Heinonen J. Estimating extreme level ice and ridge thickness for offshore wind turbine design: case study Kriegers Flak. Wind Energy 2021;25(4):639–59. https://doi.org/10.1002/we.2690.
[24] International Standard Organisation. Arctic offshore structures. ISO; 2019. 19906.
[25] Guntur S, Jonkman J, Schreck S, Jonkman B, Wang Q, Sprague M, et al. Fast v8 verification and validation for a MW-scale wind turbine with aeroelastically tailored blades. 34th Wind Energy Symp 2017:443–68. https://doi.org/10.2514/6.2016-1008.
[26] Hendrikse H, Nord TS. Dynamic response of an offshore structure interacting with an ice floe failing in crushing. Mar Struct 2019;65:271–90. https://doi.org/10.1016/j.marstruc.2019.01.012.
[27] Kärnä T, Qu Y. Analysis of the size effect in ice crushing. Technical Research Centre of Finland VTT 2009:205. Internal Report.
[28] Gagnon R. Spallation-based numerical simulations of ice-induced vibration of structures. Cold Reg Sci Technol 2021;194:23p. https://doi.org/10.1016/j.coldregions.2021.103465.
[29] Rubak R, Petersen J. Monopile as part of aeroelastic wind turbine simulation code. In: Proceedings of copenhagen offshore wind Denmark; 2005.
[30] Krenk S, Couturier PJ. Equilibrium-based nonhomogeneous anisotropic beam element. AIAA J 2017;55:2773–82. https://doi.org/10.2514/1.J055884.
[31] Couturier PJ, Skjoldan PF. Implementation of an advanced beam model in BHawC. J Phys Conf Ser 2018;1037:10p. https://doi.org/10.1088/1742-6596/1037/6/062015.
[32] Skjoldan PF. Aeroelastic modal dynamics of wind turbines including anisotropic effects. Danmarks Tek Univ Risø Natl Bæredygtig Energi. 2011. Risø-PhD.
[33] Sodhi DS. Crushing failure during ice-structure interaction. Eng Fract Mech 2001;68:1889–921. https://doi.org/10.1016/S0013-7944(01)00038-8.
[34] Määttänen M. Dynamic ice-structure interaction during continuous crushing. USA: Hanover, New Hampshire; 1983.
[35] Toyama Y, Sensu T, Minami M, Yashima N. Model tests on ice-induced self-excited vibration of cylindrical structures. In: Proc. 7th Int. Conf. Port Ocean Eng. under Arct. Cond., vol. 2; 1983. p. 834–44. Helsinki, Finland.
[36] Owen CC, Hendrikse H. A study of the transition ice speed from intermittent crushing to frequency lock-in vibrations based on model-scale experiments. In: Proc. 25th Int. Conf. Port Ocean Eng. under Arct. Cond.; 2019. p. 14.
[37] Gagnon RE. An explanation for the Molikpaq May 12, 1986 event. Cold Reg Sci Technol 2012;82:75–93. https://doi.org/10.1016/j.coldregions.2012.05.009.
[38] Nord TS, Samardžija I, Hendrikse H, Bjerkås M, Høyland KV, Li H. Ice-induced vibrations of the Norströmsgrund lighthouse. Cold Reg Sci Technol 2018;155:237–51. https://doi.org/10.1016/j.coldregions.2018.08.005.
[39] Gaertner E, Rinker J, Sethuraman L, Anderson B, Zahle F, Barter G. IEA wind TCP task 37: definition of the IEA 15 MW offshore reference wind turbine. 2020. p. 44.